Antiphase structures of an improper ferroelastic phase transition driven by an M_5^- zone boundary phonon in $RAg_{1-x}In_x$

Wenwu Cao,[1,*] Avadh Saxena,[2,†] and Dorian M. Hatch[3,‡]
[1]*Materials Research Laboratory, The Pennsylvania State University, University Park, Pennsylvania 16802*
[2]*Theoretical Division, Los Alamos National Laboratory, Los Alamos, New Mexico 87545*
[3]*Department of Physics, Brigham Young University, Provo, Utah 84602*
(Received 12 October 1999; revised manuscript received 21 February 2001; published 21 June 2001)

Rare-earth alloys $RAg_{1-x}In_x$ (where R=La, Ce, and Pr) are improper ferroelastic materials with the CsCl structure. A weakly first-order phase transition occurs with the softening of a zone-edge M_5^- mode that drives the material from a cubic phase to a tetragonal phase. Based on Ginzburg-Landau theory, we utilize the complete free-energy density, constructed from a six-dimensional primary order parameter (shuffle) that couples to strain, to study domain formation. The model allows the study of complex antiphase structures that appear in this cubic-to-tetragonal phase transition. With the help of numerical techniques, the order-parameter profiles across antiphase boundaries of different orientations and their temperature dependence are calculated. We find a single set of two coupled dimensionless governing equations, which are applicable to order-parameter profiles across all antiphase boundaries for this transition.

DOI: 10.1103/PhysRevB.64.024106 PACS number(s): 64.70.Kb, 02.20.−a, 61.50.Ah, 61.50.Ks

I. INTRODUCTION

Landau theory was originally developed for a second-order phase transition for which the amplitude of the soft-mode phonon becomes dominant near the phase-transition temperature.[1] This expansion method of using only the amplitude of the dominant mode is also applicable to the case of a weakly first-order phase transition.[2,3] To account for the inhomogeneous structures that occur as a result of the phase transition, an energy term associated with order-parameter (OP) gradients was introduced, which is often called the Ginzburg term.[4] The simple formulation of Ginzburg-Landau (GL) theory has proven to be successful for the description of many phase transitions and inhomogeneous structures, such as domains, domain walls, and interfaces.[5] In most of the cases reported in the literature, simplified one- or two-dimensional models are often used that, although easy to solve mathematically, often miss many interesting physical phenomena associated with the phase transition, such as possible lower symmetry phases and antiphase structures, which are of particular interest here.

As a general rule, the formulation of the GL free energy should be based on the symmetry relations between the parent and product phases. There are two routes of constructing the GL theory and they differ in the method of selection of the basis for the order parameter. The lattice-dynamical approach follows the idea of using the modes obtained from the diagonalization of the dynamical matrix. The amplitudes or phase angles of the relevant modes are chosen as the order parameter to describe the phase transition.[6–11] Another equivalent and convenient approach is to generate the free energy and the displacement modes from the basis vectors of irreducible representations of the space group of the parent phase. The OP then has its foundation in the symmetry relationship between the parent and product phases and the associated representation that induces the symmetry change.[12,13] It has been shown that the two formulations are equivalent and can be converted from one to the other by a rotation of basis within OP space.[14] In this paper, we use the lattice-dynamical formulation, which was also checked against the group-theoretical approach using the program ISOTROPY.[15]

The soft phonon mode in $La(Ag_{1-x}In_x)$ ($x=0.2$) has been measured by several groups.[16–18] Specifically, the transverse acoustic (TA) phonon mode of the parent phase with wave vector $\mathbf{k}=[1,1,0](\pi/a)$ and polarization in the $[1\bar{1}0]$ direction softens as the transition temperature is approached from above. This TA mode is degenerate with the longitudinal acoustic (LA) mode with wave vector $\mathbf{k}=[1,1,0](\pi/a)$ and polarization in [110]. By comparing the softening of the shear modulus $C'=(C_{11}-C_{12})/2$ and temperature dependence of other elastic constants with the TA mode softening, the conclusion is reached that the atomic shuffles are the primary cause for the transformation and the strains play a secondary role. Any softening of elastic moduli is a result of anharmonic coupling of the primary OP to the strains.

In the next section, we present the details of the free energy in terms of a six-component shuffle order parameter. We incorporate coupling of the primary OP with the strain as well as the Ginzburg (nonlocal gradient) terms. Section III describes the homogeneous solutions. In Sec. IV, the general procedure is developed for using a phonon mode order parameter in more than three dimensions (a six-component ''vector'') to describe antiphase microstructures. We present the various antiphase boundary solutions. A single set of coupled nonlinear equations that provide OP profiles for all possible antiphase domain relationships for this transition are obtained. Section V contains a brief discussion and connection to experimental data in order to determine the parameters of the Ginzburg-Landau model. Finally, we summarize the main results in Sec. VI.

II. GINZBURG-LANDAU FREE ENERGY

The materials of interest here, $R\mathrm{Ag}_{1-x}\mathrm{In}_x$ (R=La, Ce, Pr), have the CsCl structure (space group O_h^1, $Pm\bar{3}m$) with two atoms per unit cell in the cubic phase and undergo an improper ferroelastic transition to a tetragonally distorted phase (space group D_{4h}^{17}, $I4/mmm$) with primitive cell quadrupling. Using lattice dynamics, one can derive the six degenerate eigenvectors which correspond to the M_5^- mode.[14] We denote the equilibrium atomic positions by $\mathbf{x}(\mathbf{l}\kappa)=\mathbf{x}(\mathbf{l})+\mathbf{x}(\kappa)$, where $\mathbf{x}(\mathbf{l})=l_x\mathbf{a}+l_y\mathbf{b}+l_z\mathbf{c}$ and $\mathbf{x}(\kappa)=(1/2)(\kappa-1)(\mathbf{a}+\mathbf{b}+\mathbf{c})$. Here, l_α=integer ($\alpha=x,y,z$), and labels the origin of the lth unit cell in multiples of the lattice constant a; $\kappa=1,2$ denotes the two sublattices of the CsCl structure; $\mathbf{a}=a\hat{x}$, $\mathbf{b}=a\hat{y}$, and $\mathbf{c}=a\hat{z}$ are the crystallographic axes of the primitive cubic lattice. For periodic boundary conditions, all atomic displacements $\mathbf{u}(\mathbf{l}\kappa)$ from the equilibrium positions may be expanded in a Fourier series with respect to the normal coordinates $Q(\mathbf{k}\lambda)$ according to

$$u_\alpha(\mathbf{l}\kappa)=\frac{1}{\sqrt{NM_\kappa}}\sum_{\mathbf{k}\lambda} e_\alpha(\kappa|\mathbf{k}\lambda)\ e^{i\mathbf{k}\cdot\mathbf{x}(\mathbf{l})}Q(\mathbf{k}\lambda),$$

where M_κ ($\kappa=1,2$) denotes the masses of the two types of atoms and the sum is extended over all wave vectors $\mathbf{k}$ of the first Brillouin zone and over all branches λ ($=1,2,\ldots,6$ for the CsCl structure) of the associated phonon-dispersion curves. The expansion coefficients $e_\alpha(\kappa|\mathbf{k}\lambda)$ are the eigenvectors of the dynamical matrix. Thus, from the orthonormality of $e_\alpha(\kappa|\mathbf{k}\lambda)$,

$$Q(\mathbf{k}\lambda)=\frac{1}{\sqrt{N}}\sum_{\alpha l\kappa}\sqrt{M_\kappa}e_\alpha^*(\kappa|\mathbf{k}\lambda)u_\alpha(\mathbf{l}\kappa)e^{-i\mathbf{k}\cdot\mathbf{x}(\mathbf{l})}.$$

The primary OP driving the transition here is a softening M_5^- phonon mode and consists of the set of normal mode coordinates $\mathbf{Q}=(Q_1,Q_2,Q_3,Q_4,Q_5,Q_6)$ that belong to the star of the wave vector $\mathbf{k}$ at the M point. The $\mathbf{k}_M$ star has three arms and the mode corresponding to each arm of the star has twofold degeneracy. The Q_i's are given by

$$\begin{aligned}
Q_1&=\sum_{L=1}^{8}[u_0u_x(L)+v_0v_y(L)](-1)^{l_x+l_y},\\
Q_2&=\sum_{L=1}^{8}[u_0u_y(L)+v_0v_x(L)](-1)^{l_x+l_y},\\
Q_3&=\sum_{L=1}^{8}[u_0u_z(L)+v_0v_x(L)](-1)^{l_x+l_z},\\
Q_4&=\sum_{L=1}^{8}[u_0u_x(L)+v_0v_z(L)](-1)^{l_x+l_z},
\end{aligned}\tag{1}$$

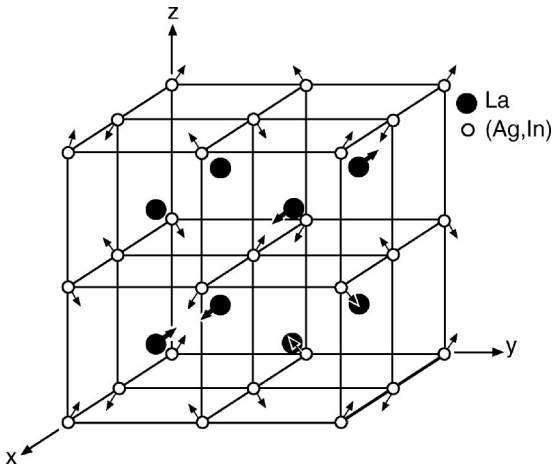

FIG. 1. Doubly extended CsCl structure with atomic displacements in I_x domain state.

$$\begin{aligned}
Q_5&=\sum_{L=1}^{8}[u_0u_y(L)+v_0v_z(L)](-1)^{l_y+l_z},\\
Q_6&=\sum_{L=1}^{8}[u_0u_z(L)+v_0v_y(L)](-1)^{l_y+l_z},
\end{aligned}$$

where $\mathbf{u}$ and $\mathbf{v}$ are the normalized displacements of the two sublattices $\mathrm{In}_{1-x}\mathrm{Ag}_x$ and La, respectively, and the summation is over eight parent primitive unit cells ($2\times2\times2$) labeled by L which make up the supercell required by M_5^- (see Fig. 1). Furthermore,

$$u_0=\sqrt{\frac{M_1}{8}}u_1,\qquad v_0=\sqrt{\frac{M_2}{8}}v_1;$$

$$u_1=-\sqrt{\frac{M_1}{M_1+\zeta^2M_2}},\qquad v_1=\sqrt{\frac{\zeta^2M_2}{M_1+\zeta^2M_2}},$$

where the parameter ζ depends on the interatomic force constants of the relevant mode, and M_1 and M_2 denote the masses of the two types of atoms ($\mathrm{In}_{1-x}\mathrm{Ag}_x$ and La) in the unit cell (see Fig. 1). The quantities u_1 and v_1 appear in Eq. (10) below (Sec. III) where atomic displacements are expressed in terms of the normal mode amplitudes Q_i.

Using the above six eigenvectors and the O_h^1 space group symmetry operations, the total GL free-energy density can be written in the following form:[15]

$$F=F_L+F_{\mathrm{el}}+F_c+F_G,\tag{2}$$

where the Landau free energy, F_L, contains the primary OP contributions from the M_5^- normal mode coordinates,

$$
\begin{aligned}
F_L = {} & A(Q_1^2+Q_2^2+Q_3^2+Q_4^2+Q_5^2+Q_6^2)+B_1(Q_1^2+Q_2^2+Q_3^2+Q_4^2+Q_5^2+Q_6^2)^2 \\
& +B_2(Q_1^2Q_3^2+Q_1^2Q_5^2+Q_3^2Q_5^2+Q_2^2Q_4^2+Q_2^2Q_6^2+Q_4^2Q_6^2)+B_3(Q_1^2Q_4^2+Q_2^2Q_5^2+Q_3^2Q_6^2)+B_4(Q_1^2Q_6^2+Q_2^2Q_3^2+Q_4^2Q_5^2) \\
& +B_5(Q_1^2Q_2^2+Q_3^2Q_4^2+Q_5^2Q_6^2)+C_1(Q_1^2+Q_2^2+Q_3^2+Q_4^2+Q_5^2+Q_6^2)^3 \\
& +C_2(Q_1^2+Q_2^2+Q_3^2+Q_4^2+Q_5^2+Q_6^2)(Q_1^2Q_3^2+Q_1^2Q_5^2+Q_3^2Q_5^2+Q_2^2Q_4^2+Q_2^2Q_6^2+Q_4^2Q_6^2) \\
& +C_3(Q_1^2+Q_2^2+Q_3^2+Q_4^2+Q_5^2+Q_6^2)(Q_1^2Q_4^2+Q_2^2Q_5^2+Q_3^2Q_6^2) \\
& +C_4(Q_1^2+Q_2^2+Q_3^2+Q_4^2+Q_5^2+Q_6^2)(Q_1^2Q_6^2+Q_2^2Q_3^2+Q_4^2Q_5^2) \\
& +C_5(Q_1^2+Q_2^2+Q_3^2+Q_4^2+Q_5^2+Q_6^2)(Q_1^2Q_2^2+Q_3^2Q_4^2+Q_5^2Q_6^2) \\
& +C_6[(Q_1^2+Q_2^2-Q_3^2-Q_4^2)(Q_1^2Q_5^2+Q_2^2Q_6^2-Q_3^2Q_5^2-Q_4^2Q_6^2)+(Q_5^2+Q_6^2-Q_1^2-Q_2^2)(Q_3^2Q_5^2+Q_4^2Q_6^2-Q_1^2Q_3^2-Q_2^2Q_4^2) \\
& +(Q_3^2+Q_4^2-Q_5^2-Q_6^2)(Q_1^2Q_3^2+Q_2^2Q_4^2-Q_1^2Q_5^2-Q_2^2Q_6^2)] \\
& +C_7[(Q_1^4-Q_4^4)(Q_2^2+Q_5^2-Q_3^2-Q_6^2)+(Q_2^4-Q_5^4)(Q_1^2+Q_4^2-Q_3^2-Q_6^2)+(Q_3^4-Q_6^4)(Q_1^2+Q_4^2-Q_2^2-Q_5^2)] \\
& +C_8[(Q_1^4-Q_6^4)(Q_2^2+Q_3^2-Q_4^2-Q_5^2)+(Q_2^4-Q_3^4)(Q_1^2+Q_6^2-Q_4^2-Q_5^2)+(Q_4^4-Q_5^4)(Q_2^2+Q_3^2-Q_1^2-Q_6^2)] \\
& +C_9[(Q_1^4-Q_2^4)(Q_3^2+Q_4^2-Q_5^2-Q_6^2)+(Q_3^4-Q_4^4)(Q_5^2+Q_6^2-Q_1^2-Q_2^2)+(Q_5^4-Q_6^4)(Q_1^2+Q_2^2-Q_3^2-Q_4^2)] \\
& +C_{10}(Q_1Q_2Q_3Q_4Q_5Q_6)+C_{11}[(Q_3+Q_4)^2\{(Q_1+Q_2)^2(Q_5+Q_6)^2+(Q_2-Q_1)^2(Q_6-Q_5)^2\} \\
& +(Q_4-Q_3)^2\{(Q_1+Q_2)^2(Q_6-Q_5)^2+(Q_2-Q_1)^2(Q_5+Q_6)^2\}]. \qquad (3a)
\end{aligned}
$$

F_{el} contains the secondary OP elastic contribution [see the definitions of the strains in Eqs. (4a)–(4f) below],

$$F_{\mathrm{el}}=\frac{\hat{c}_{11}}{2}e_1^2+\frac{\hat{c}_{22}}{2}(e_2^2+e_3^2)+\frac{\hat{c}_{44}}{2}(e_4^2+e_5^2+e_6^2). \qquad (3b)$$

F_c contains terms that couple the phonon modes with the elastic strains,

$$
\begin{aligned}
F_c = {} & D_1e_1(Q_1^2+Q_2^2+Q_3^2+Q_4^2+Q_5^2+Q_6^2) \\
& +D_2[\sqrt{3}e_2(Q_5^2+Q_6^2-Q_3^2-Q_4^2) \\
& +e_3(Q_3^2+Q_4^2+Q_5^2+Q_6^2-2Q_1^2-2Q_2^2)] \\
& +D_3[e_2\{(Q_4^2-Q_3^2)+(Q_6^2-Q_5^2)-2(Q_2^2-Q_1^2)\} \\
& +\sqrt{3}e_3\{(Q_4^2-Q_3^2)-(Q_6^2-Q_5^2)\}] \\
& +D_4(e_4Q_5Q_6+e_5Q_3Q_4+e_6Q_1Q_2). \qquad (3c)
\end{aligned}
$$

The gradient (or Ginzburg) energy F_G, with a subscript preceded by a comma denoting partial differentiation, is given by[19]

$$
\begin{aligned}
F_G = {} & g_1(Q_{4,x}^2+Q_{3,z}^2+Q_{1,x}^2+Q_{2,y}^2+Q_{5,y}^2+Q_{6,z}^2) \\
& +g_2(Q_{3,x}^2+Q_{4,z}^2+Q_{2,x}^2+Q_{1,y}^2+Q_{6,y}^2+Q_{5,z}^2) \\
& +g_3(Q_{1,z}^2+Q_{2,z}^2+Q_{3,y}^2+Q_{4,y}^2+Q_{5,x}^2+Q_{6,x}^2) \\
& +g_4(Q_{3,x}Q_{4,z}+Q_{1,y}Q_{2,x}+Q_{5,z}Q_{6,y}) \\
& +g_5(Q_{3,z}Q_{4,x}+Q_{1,x}Q_{2,y}+Q_{5,y}Q_{6,z}). \qquad (3d)
\end{aligned}
$$

The OP gradient terms describe the generalized ''exchange'' interaction between neighboring domains in a material with spatially varying OP.

The symmetry-adapted strain tensor components e_i are defined in terms of the conventional (geometrically linear) strain $\varepsilon_{ij}=\frac{1}{2}[(\partial u_i/\partial x_j)+(\partial u_j/\partial x_i)]$ by the following relations:

$$e_1=\frac{1}{\sqrt{3}}(\varepsilon_{xx}+\varepsilon_{yy}+\varepsilon_{zz}), \qquad (4a)$$

$$e_2=\frac{1}{\sqrt{2}}(\varepsilon_{xx}-\varepsilon_{yy}), \qquad (4b)$$

$$e_3=\frac{1}{\sqrt{6}}(\varepsilon_{xx}+\varepsilon_{yy}-2\varepsilon_{zz}), \qquad (4c)$$

$$e_4=\varepsilon_{xy}, \qquad (4d)$$

$$e_5=\varepsilon_{yz}, \qquad (4e)$$

$$e_6=\varepsilon_{xz}, \qquad (4f)$$

and the elastic constants $\hat{c}_{ij}$ are given by

$$\hat{c}_{11}=c_{11}+2c_{12}, \qquad (4g)$$

$$\hat{c}_{22}=c_{11}-c_{12}, \qquad (4h)$$

$$\hat{c}_{44}=4c_{44}. \qquad (4i)$$

TABLE I. Homogeneous solutions corresponding to the tetragonal product phase.

Tetragonal axis	Domain No.	Tetragonal state	Order parameter	Displacement direction of the atom at $x(\kappa)=[0,0,0]a$	Displacement direction of the atom at $x(\kappa)=1/2[1,1,1]a$
x	3	I_x	$(0,Q_0,Q_0,0,0,0)$	$[011]$	$[100]$
	6	II_x	$(0,-Q_0,Q_0,0,0,0)$	$[0\bar{1}1]$	Not moving
	9	III_x	$(0,Q_0,-Q_0,0,0,0)$	$[01\bar{1}]$	Not moving
	12	IV_x	$(0,-Q_0,-Q_0,0,0,0)$	$[0\bar{1}\bar{1}]$	$[\bar{1}00]$
y	2	I_y	$(Q_0,0,0,0,0,Q_0)$	$[101]$	$[010]$
	5	II_y	$(Q_0,0,0,0,0,-Q_0)$	$[10\bar{1}]$	Not moving
	8	III_y	$(-Q_0,0,0,0,0,Q_0)$	$[\bar{1}01]$	Not moving
	11	IV_y	$(-Q_0,0,0,0,0,-Q_0)$	$[\bar{1}0\bar{1}]$	$[0\bar{1}0]$
z	1	I_z	$(0,0,0,-Q_0,-Q_0,0)$	$[110]$	$[001]$
	4	II_z	$(0,0,0,-Q_0,Q_0,0)$	$[\bar{1}10]$	Not moving
	7	III_z	$(0,0,0,Q_0,-Q_0,0)$	$[1\bar{1}0]$	Not moving
	10	IV_z	$(0,0,0,-Q_0,-Q_0,0)$	$[\bar{1}\bar{1}0]$	$[00\bar{1}]$

Note that the shear strains $e_4=e_5=e_6=0$ for the cubic-to-tetragonal transition. Only the gradient energy of the primary OP is considered here and the elastic energy is kept only up to the second order in strain. All energy expansion coefficients are assumed to be temperature-independent except $A=\alpha_0(T-T_c)$. Here T_c is the (fictitious) temperature at which the mode frequency would become zero. The Landau portion, F_L, of the free energy is essentially the same as that obtained in Ref. 14. (Note that the 11th invariant of the sixth degree [see Eq. (3a) in Sec. II] was inadvertently left out in Tables 4a and 4b of this reference.) The Ginzburg terms, F_G, were not contained in that reference and are important contributions to the description of antiphase domains, as we will see in Sec. IV below.

III. HOMOGENEOUS SOLUTIONS

For a homogeneous system, the gradient energy contribution vanishes so that the solutions are determined by minimizing the free energy of the first three terms in Eq. (2). Using the variational technique, one can derive the Euler-Lagrange equations, which are six coupled partial differential equations in Q_i and six more equations for the elastic strain,

$$\sum_m \frac{\partial}{\partial x_m}\left[\frac{\partial F}{\partial Q_{i,m}}\right]-\frac{\partial F}{\partial Q_i}=0, \tag{5a}$$

$$\sum_{m,\lambda}\frac{\partial}{\partial x_m}\left(\frac{\partial F}{\partial e_\lambda}\frac{\partial e_\lambda}{\partial \varepsilon_{im}}\right)=0 \quad (m=1,2,3;\ i,\lambda=1,2,\ldots,6). \tag{5b}$$

Define $\sigma_\lambda=\partial F/\partial e_\lambda$ to be the generalized stress tensor corresponding to the strain definition of Eq. (4). Then,

$$\sigma_1=\hat{c}_{11}e_1+D_1(Q_1^2+Q_2^2+Q_3^2+Q_4^2+Q_5^2+Q_6^2), \tag{6a}$$

$$\sigma_2=\hat{c}_{22}e_2+\sqrt{3}D_2(Q_5^2+Q_6^2-Q_3^2-Q_4^2)+\sqrt{3}D_3(Q_1^2+Q_4^2-Q_2^2-Q_5^2), \tag{6b}$$

$$\sigma_3=\hat{c}_{22}e_3+D_2(Q_3^2+Q_4^2+Q_5^2+Q_6^2-2Q_1^2-2Q_2^2)+D_3(Q_1^2+Q_2^2+Q_4^2+Q_5^2-2Q_3^2-2Q_6^2), \tag{6c}$$

$$\sigma_4=\hat{c}_{44}e_4+D_4Q_5Q_6, \tag{6d}$$

$$\sigma_5=\hat{c}_{44}e_5+D_4Q_3Q_4, \tag{6e}$$

$$\sigma_6=\hat{c}_{44}e_6+D_4Q_1Q_2. \tag{6f}$$

In a homogeneous phase, the stress is zero everywhere, i.e., $\sigma_\lambda=0$, therefore, for equilibrium single domain states, the six strain components e_i can be expressed in terms of the six order-parameter components Q_i. These expressions for strain are then substituted back into $F_{\rm el}$ and F_c. As a result, we obtain an effective free energy just of the form F_L in Eq. (3a), with ''renormalized'' coefficients. Minima of this effective free energy yield lower symmetry domain states.

There are twelve single domain states for our tetragonal phase. These are given in Table I in terms of the OP vector $\mathbf{Q}=(Q_1,Q_2,Q_3,Q_4,Q_5,Q_6)$. As shown in Table I, four degenerate states exist for each of the three principal tetragonal axes. We label these solutions by a domain number (from ISOTROPY[15]) and by a capital Roman numeral letter with a subscript indicating the corresponding tetragonal axis.

For a first-order transition the expansion must be at least to sixth degree (in the absence of third order invariants). The transition temperature T_0 and the spontaneous OP value Q_c (at T_0) are given by

$$T_0=T_c+\frac{b^2}{16\alpha_0(4C_1+C_4-C_7-C_9)}, \tag{7a}$$

$$Q_c^2 = -\frac{b}{4(4C_1 + C_4 - C_7 - C_9)}, \tag{7b}$$

where

$$b = 4B_1 + B_4 - \left[\frac{4D_1^2}{\hat{c}_{11}} + \frac{4}{\hat{c}_{22}}(D_2 + \sqrt{3}D_3)^2\right]. \tag{8}$$

For other temperatures below T_0, the amplitude of the OP, Q_0, in a single tetragonal domain state can be related to Q_c through the following relation:

$$Q_0 = Q_c \sqrt{\frac{2}{3}\left(1 + \sqrt{1 - \frac{3}{4}\tau}\right)}, \tag{9a}$$

$$\tau = \frac{T - T_c}{T_0 - T_c}. \tag{9b}$$

The normal mode amplitude Q_0 is linked to the atomic displacement of the two atoms through Eq. (1). Since we are working in the Q space, it is useful to invert Eq. (1),

$$u_x^{(L)} = (u_1/\sqrt{8M_1})[(-1)^{l_x+l_y}\ Q_1 + (-1)^{l_x+l_z}\ Q_4], \tag{10a}$$

$$u_y^{(L)} = (u_1/\sqrt{8M_1})[(-1)^{l_x+l_y}\ Q_2 + (-1)^{l_y+l_z}\ Q_5], \tag{10b}$$

$$u_z^{(L)} = (u_1/\sqrt{8M_1})[(-1)^{l_x+l_z}\ Q_3 + (-1)^{l_y+l_z}\ Q_6], \tag{10c}$$

$$v_x^{(L)} = (v_1/\sqrt{8M_2})[(-1)^{l_x+l_y}\ Q_2 + (-1)^{l_x+l_z}\ Q_3], \tag{10d}$$

$$v_y^{(L)} = (v_1/\sqrt{8M_2})[(-1)^{l_x+l_y}\ Q_1 + (-1)^{l_y+l_z}\ Q_6], \tag{10e}$$

$$v_z^{(L)} = (v_1/\sqrt{8M_2})[(-1)^{l_x+l_z}\ Q_4 + (-1)^{l_y+l_z}\ Q_5]. \tag{10f}$$

Here $u_i^{(L)}$ and $v_i^{(L)}$ are displacement components of the two sublattices at [0,0,0] and $[a/2,a/2,a/2]$, respectively. The superscript, $L = 1,2,\ldots,8$, represents labeling of the unit cells which make up our expanded supercell (see Fig. 1).

The last two columns of Table I give the lattice displacement direction for the two atoms in the unit cell that is located at the origin of our coordinate system. One can easily generate the lattice displacement pattern for the supercell from the pattern of the first cell together with Eq. (10). For example, for domain state I_x, the three-dimensional lattice displacement pattern is shown in Fig. 1 and the pattern for I_z was given in Fig. 1 of Ref. 14.

Since the three-dimensional respresentation is difficult to plot unambiguously, it is useful to use the 2D projection of these states. Shown in Fig. 2(a) is the projection plot on the $z = 0$ plane for the domain state I_x. There are four such domain states having the tetragonal axis in the x direction. The dot (cross) in the center of a lattice circle represents that the lattice point also moves up (down) at the same time as it moves along the arrow direction in the plane in the low-temperature phase. The shaded lattice in the center of the unit cell is half a unit higher above the base plane, i.e., at the $z = a/2$ plane. The displacement patterns for II_x, III_x, and IV_x can be obtained by a translation of the coordinate system by a vector of $[0,a,0]$, $[a,0,0]$, and $[a,a,0]$, respectively. Figures 2(b) and 2(c) correspond to domain states I_y and I_z, respectively, with other patterns (II_y,III_y,IV_y and II_z,III_z,IV_z) obtained via translation by appropriate vectors.

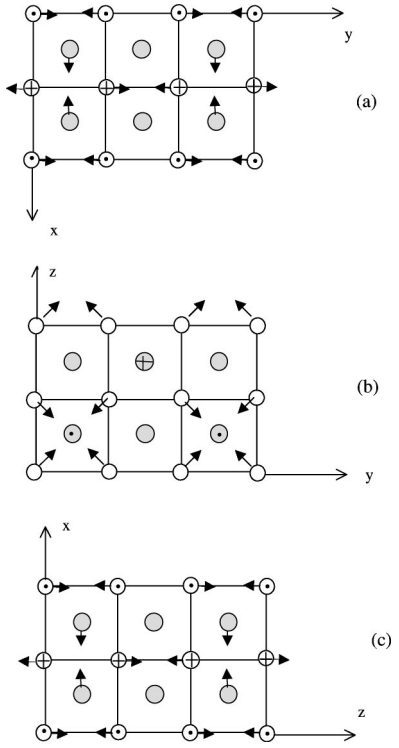

FIG. 2. 2D projection of lattice displacement patterns (a) on the $z = 0$ plane with tetragonal axis in the x direction for domain state I_x, (b) on the $x = 0$ plane with tetragonal axis in the y direction for domain state I_y, and (c) on the $y = 0$ plane with tetragonal axis in the z direction for domain state I_z.

IV. ANTIPHASE BOUNDARY SOLUTIONS

The existence of four variants for each tetragonal orientation, related by a fractional translation (which is not a body center point, i.e., [1/2,1/2,1/2]) of the new structure, will create antiphase variant structures. An antiphase boundary (APB) is the (planar or curved) surface where two such domain states meet. We choose the first group of solutions in Table I as examples for the analysis. Antiphase structures allow different domain relationships to form, distinct from ferroelastic domains, since the requirement of strain compatibility is automatically satisfied. A few special orientations of the APBs are studied here to illustrate the associated richness of the atomic structure and the corresponding continuum description of the antiphase boundaries. For mathematical simplicity, we will only study planar APBs so that the problem can be rendered quasi-one-dimensional for each given antiphase structure.

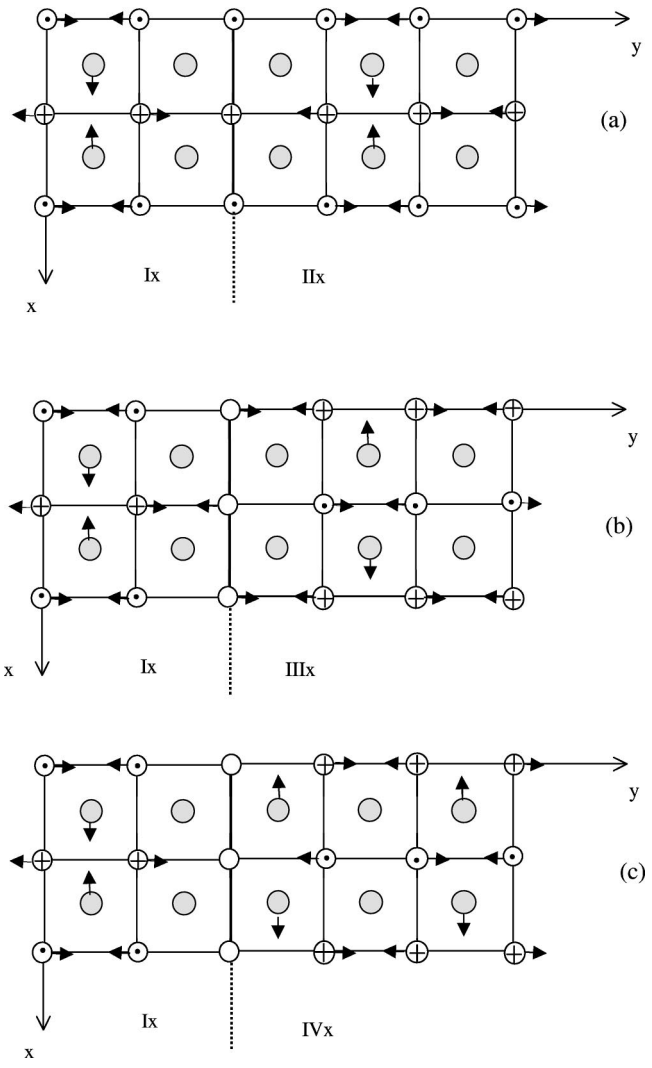

FIG. 3. Illustration of lattice displacement pattern in three different antiphase structures with APBs oriented along the *y* direction: (a) I_x-II_x, (b) I_x-III_x, and I_x-IV_x.

A. Antiphase boundary oriented along [010]

As examples we take the four domain states given in Table I, with the tegragonal axis along the *x* direction. APBs can orient in many directions, for example with normals, [100], [010], [110], [011], etc. Any two of the four states can be paired up with an APB along these orientations. For simplicity, let us first study the case of the APB oriented along [010]. A few combinations of antiphase structures are I_x-II_x, I_x-III_x, and I_x-IV_x as shown in Figs. 3(a)–3(c). At the I_x-II_x antiphase boundary, the $Ag_{1-x}In_x$ atoms shift along the *z* direction; for the case of the I_x-III_x antiphase boundary, the $Ag_{1-x}In_x$ atoms shift along the *y* direction; while for the case of the I_x-IV_x antiphase boundary, the $Ag_{1-x}In_x$ atoms stay put.

Under the quasi-1D (Q1D) approximation, the physical quantities are a function of space variable *y* only and only two components Q_2 and Q_3 are nonzero. Therefore, $\mathbf{Q}=(0,Q_2(y),Q_3(y),0,0,0)$. From Eq. (5a), we have

$$\begin{aligned} g_1Q_{2,yy}=&AQ_2+2B_1Q_2(Q_2^2+Q_3^2)+B_4Q_2Q_3^2\\ &+3C_1Q_2(Q_2^2+Q_3^2)^2\\ &+(C_4-C_7-C_9)(2Q_2^2+Q_3^2)Q_2Q_3^2+D_1e_1Q_2\\ &-2D_2e_3Q_2+D_3(e_3-\sqrt{3}e_2)Q_2, \end{aligned} \tag{11a}$$

$$\begin{aligned} g_3Q_{3,yy}=&AQ_3+2B_1Q_3(Q_2^2+Q_3^2)+B_4Q_3Q_2^2\\ &+3C_1Q_3(Q_2^2+Q_3^2)^2\\ &+(C_4-C_7-C_9)(2Q_3^2+Q_2^2)Q_3Q_2^2+D_1e_1Q_3\\ &-2D_3e_3Q_3+D_2(e_3-\sqrt{3}e_2)Q_3. \end{aligned} \tag{11b}$$

The boundary conditions determine which particular APB pair of the four domain states is described by the solutions of Eq. (11). For the II_x-I_x antiphase structure,

$$\lim_{y\to\pm\infty}(Q_2,Q_3)=(\pm Q_0,Q_0); \tag{12a}$$

for the III_x-I_x antiphase structure,

$$\lim_{y\to\pm\infty}(Q_2,Q_3)=(Q_0,\pm Q_0); \tag{12b}$$

and for the IV_x-I_x antiphase structure,

$$\lim_{y\to\pm\infty}(Q_2,Q_3)=(\pm Q_0,\pm Q_0). \tag{12c}$$

In order to solve for a general case, we follow the procedure of Refs. 10,11 and 20 to normalize the order parameter and define

$$\begin{aligned} A'=&D_1e_1^\infty-2(D_2+\sqrt{3}D_3)e_3^\infty\\ &+\frac{[\sqrt{2}D_1-2(D_2-\sqrt{3}D_3)](\sqrt{2}D_1+D_2+\sqrt{3}D_3)}{\hat{c}_{11}+2\hat{c}_{22}}Q_0^2, \end{aligned} \tag{13a}$$

$$B_1'=-\frac{(\sqrt{2}D_1-2D_2+2\sqrt{3}D_3)^2}{4(\hat{c}_{11}+2\hat{c}_{22})}, \tag{13b}$$

$$B_4'=\frac{[\sqrt{2}D_1-2(D_2-\sqrt{3}D_3)](\sqrt{2}D_1+4D_2)}{2(\hat{c}_{11}+2\hat{c}_{22})}, \tag{13c}$$

$$\begin{aligned} A''=&D_1e_1^\infty-2(D_2+\sqrt{3}D_3)e_3^\infty\\ &+\left[\frac{(\sqrt{2}D_1+4D_2)(\sqrt{2}D_1+D_2+\sqrt{3}D_3)}{\hat{c}_{11}+2\hat{c}_{22}}\right]Q_0^2, \end{aligned} \tag{14a}$$

$$B_1''=\frac{(\sqrt{2}D_1+4D_2)^2}{4(\hat{c}_{11}+2\hat{c}_{22})}, \tag{14b}$$

$$B_4''=B_4'. \tag{14c}$$

Using these definitions, the equilibrium conditions of Eq. (11) become

$$g_1 Q_{2,yy} = (A+A')Q_2 + 2(B_1+B_1')Q_2^3 + (2B_1+B_4+B_4')Q_2Q_3^2 + 3C_1Q_2(Q_2^2+Q_3^2)^2 + (C_4-C_7-C_9)(2Q_2^3Q_3^2+Q_2Q_3^4), \quad (15a)$$

$$g_3 Q_{3,yy} = (A+A'')Q_3 + 2(B_1+B_1'')Q_3^3 + (2B_1+B_4+B_4'')Q_3Q_2^2 + 3C_1Q_3(Q_2^2+Q_3^2)^2 + (C_4-C_7-C_9)(2Q_3^3Q_2^2+Q_3Q_2^4). \quad (15b)$$

Now, we define dimensionless functions q_1, q_2 and space variable ξ as the following:

$$(Q_2, Q_3) = Q_c(q_2, q_3), \quad (16a)$$

$$y = \gamma\xi, \quad (16b)$$

$$\gamma^2 = \frac{\sqrt{g_1 g_3}}{A_c}, \quad (16c)$$

where $A_c = \alpha_0(T_0 - T_c)$.

The final dimensionless equations are

$$dq_{2,\xi\xi} = \tau_2 q_2 - \alpha_2 q_2^3 - \alpha_2' q_2 q_3^2 + \beta q_2^5 + \left(1-\frac{\beta}{3}\right)(2q_2^3q_3^2 + q_2q_3^4), \quad (17a)$$

$$\frac{1}{d}q_{3,\xi\xi} = \tau_3 q_3 - \alpha_3 q_3^3 - \alpha_3' q_3 q_2^2 + \beta q_3^5 + \left(1-\frac{\beta}{3}\right)(2q_3^3q_2^2 + q_3q_2^4). \quad (17b)$$

Similarly, one can normalize the boundary conditions, Eq. (12). The dimensionless parameters in Eq. (17) are given by

$$\tau_2 = \tau + \frac{A'}{A_c}, \quad (18a)$$

$$\alpha_2 = \frac{8(B_1+B_1')}{b}, \quad (18b)$$

$$\alpha_2' = \frac{4(2B_1+B_4+B_4')}{b}, \quad (18c)$$

$$\tau_3 = \tau + \frac{A''}{A_c}, \quad (18d)$$

$$\alpha_3 = \frac{8(B_1+B_1'')}{b}, \quad (18e)$$

$$\alpha_3' = \frac{4(2B_1+B_4+B_4'')}{b}, \quad (18f)$$

$$d = \sqrt{\frac{g_1}{g_3}}, \quad (18g)$$

$$\beta = \frac{3C_1}{4C_1+C_4-C_7-C_9}, \quad (18h)$$

where the parameter b is given in Eq. (8). The equilibrium values for q_2, q_3 are

$$|q_2^\infty| = |q_3^\infty| = \sqrt{\frac{2}{3}\left(1+\sqrt{1-\frac{3}{4}\tau}\right)} = q_0. \quad (19)$$

We find that Eq. (17) becomes identical to the case solved in Ref. 11. Solving Eq. (17) under different boundary conditions, given by Eq. (12), gives us three different antiphase structures for $I_x - II_x$, $I_x - III_x$, and $I_x - IV_x$ with the APB oriented in [010]. The solutions for the choice of $d=1$, $\tau=-4$, $\tau_1=\tau_2=-4.1$, $\alpha_2=\alpha_3=2.1$, $\alpha_2'=\alpha_3'=1.8$, and $\beta=10$ are given in Figs. 4–6.

In Fig. 4, we depict the antiphase boundary solutions in terms of (q_2, q_3) for the three different boundary conditions. Figure 4(a) shows that q_2 is a kinklike and q_3 is a bell-like soliton for the $I_x - II_x$ antiphase structure. For the $I_x - III_x$ antiphase structure [Fig. 4(b)] the roles are reversed, i.e., q_2 is a bell-like and q_3 is a kinklike soliton. In Figs. 4(c) and 4(d), both q_2 and q_3 profiles are kinklike for the $I_x - IV_x$ antiphase structure. The difference depicted in these figures is that in Fig. 4(c), the two solutions overlap because we assumed no coupling between q_2 and q_3, i.e., $\alpha_2=\alpha_3=0$ and $\beta=0$. In general, the two kinks do not overlap as shown in Fig. 4(d) due to the cross coupling between q_2 and q_3.

Figure 5 shows the influence of the gradient coefficient, d, on the order-parameter profiles for the $I_x - II_x$ antiphase structure. In general, domain-wall thickness monotonically increases with d. Figure 6 depicts the effect of the variation in the sixth-order coefficient β. An APB becomes narrower with increasing β. In addition, the bell-like order-parameter profile flips to a hump shape at a critical value of β. Figure 7 shows the effect of temperature, τ, on the shape and amplitude of $I_x - II_x$ APB. It reveals that as temperature decreases, the amplitude of the order parameter increases while the thickness of the APB decreases.

The discontinuous atomic displacement patterns corresponding to the three different boundary conditions, Eqs. (12a)–(12c), are given in Fig. 3. Because of the constraints of the gradient energy, the actual displacement pattern changes continuously as shown by the continuum profiles of q_2 and q_3 in Figs. 4–7.

B. Antiphase boundaries of other orientations

Because the elastic strains are compatible in antiphase structures, there are several possible orientations for the antiphase boundary corresponding to certain lattice planes. The discontinuous lattice displacement patterns for antiphase structures with APBs on the (011) and (101) lattice planes are illustrated in Fig. 8.

For antiphase structures consisting of domain states with the x direction as the tetragonal axis, the order-parameter

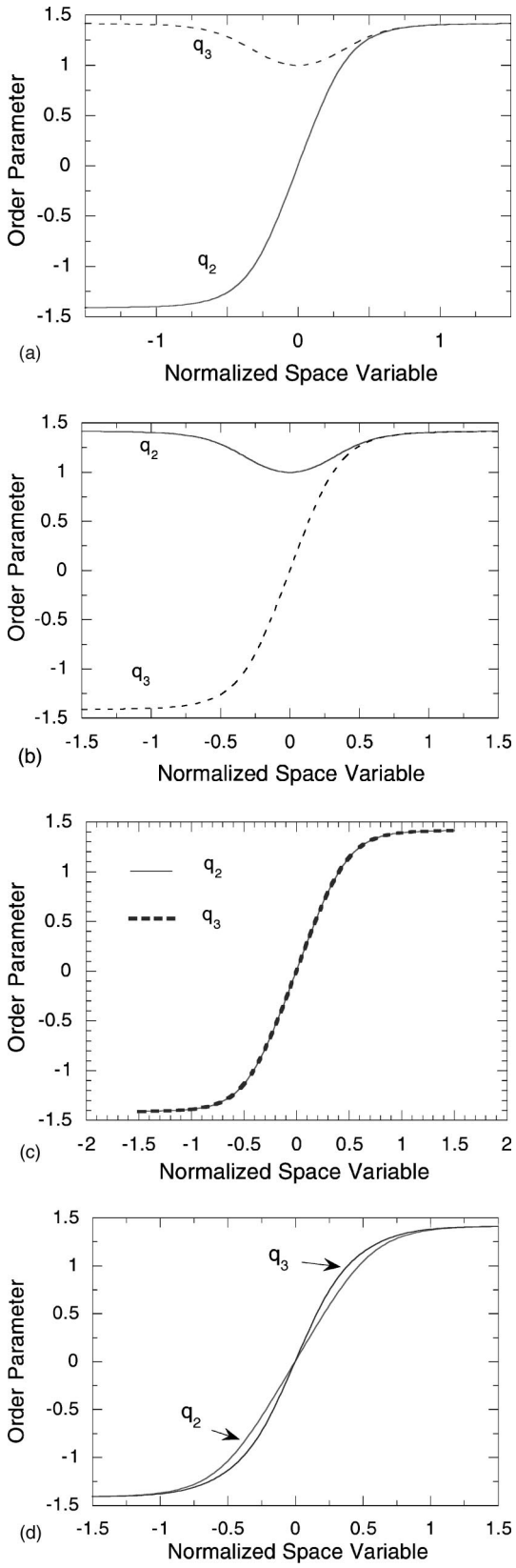

FIG. 4. Continuous order-parameter profiles for the three different antiphase structures illustrated in Fig. 3: (a) I_x-II_x, (b) I_x-III_x, (c) I_x-IV_x without coupling between q_2 and q_3, and (d) I_x-IV_x with the coupling between q_2 and q_3. The domain state on the right hand side is I_x.

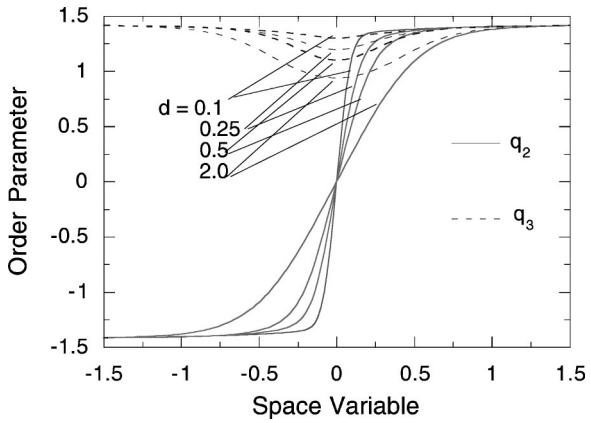

FIG. 5. Effect of the gradient coefficient d on the order-parameter profiles of the antiphase structure between I_x and II_x with APB oriented in [010].

profile is governed by two coupled differential equations for Q_2 and Q_3 as in Eqs. (15a) and (15b). The only difference is in the parameters A',A'',B_1',B_1'',B_4', and B_4''. These parameters are given in Table II for different APB orientations and are determined by material properties.

After normalization, all equations have the identical dimensionless form of Eqs. (17a) and (17b). Therefore, Eqs. (17a) and (17b) are *universal equations* for antiphase boundaries in this transition. One point that must be emphasized is that the Q1D treatment should always choose the independent space variable to be perpendicular to the APB plane. For example, while calculating the antiphase structures with APB oriented in [011] and [101], the system must be rotated 45 degrees around [100] and [010], respectively, so that the problem can be rendered Q1D.

In general, the existence of several allowed orientations for APB in a variety of materials and their relatively small energy makes it difficult to maintain the APB on one of the lattice planes through an entire sample. Instead, APBs are often observed[21–23] as curved or jointed boundaries resulting from several differently oriented APBs joining together. Moreover, the thickness of the domain wall can be on the

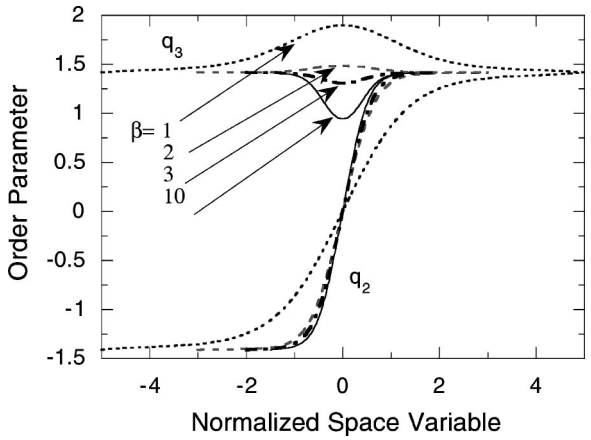

FIG. 6. Effect of the six degree energy expansion coefficient β on the order-parameter profiles of the antiphase structure between I_x and II_x with APB oriented in [010].

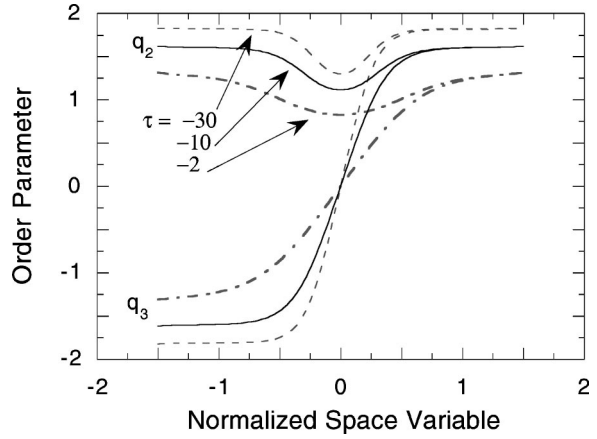

FIG. 7. Temperature dependence of the order-parameter profiles across the antiphase structure between I_x and II_x with APB oriented in [010].

order of a fraction of a unit cell to several unit cells. In simulations[23] for lead phosphate, the trace of the APB was on the same order as the ''*W*'' wall.

V. DETERMINATION OF THE EXPANSION COEFFICIENTS

The coefficients of the Landau portion of the free energy can be determined from the available lattice parameter data measured by x-ray and neutron scattering as a function of temperature. The coefficients of the Ginzburg (i.e., gradient) terms are obtained from the phonon-dispersion data near the soft mode M_5^- as described below. There is only a limited amount of data for this transition, primarily contained in Refs. 17 and 18.

A. Coefficients for the Landau energy

For the cubic-to-tetragonal transition, we have expanded the free energy to the sixth degree. The form for the effective free energy is $F_L = A(T)Q^2 + BQ^4 + CQ^6$, where $A(T) = \alpha_0(T - T_c) = m\omega_M^2$ and $m = 923.39$ kg/m^3 is the mass density. The coefficients α_0 and T_c can be determined from the temperature dependence of the soft phonon mode (Fig. 6 in Ref. 17). T_c is the temperature at which the frequency of the softening phonon would go to zero and α_0 is the slope of the linear approach to zero. T_0 is the temperature at which the first-order transition takes place. For $LaAg_{1-x}In_x$ ($x \simeq 0.2$), the cubic lattice parameter (at 300 K) is $a_c = 7.65$ Å, and the tetragonal lattice parameters (at 100 K) are $a_t = 7.56$ Å and $c_t = 7.75$ Å. In the tetragonal phase at 100 K, the shuffle (in units of the cubic lattice parameter) of La atoms is $\epsilon = 0.0285$ and the shuffle of $Ag_{1-x}In_x$ atoms is $\delta = 0.0139$ (Fig. 4 in Ref. 17). We find the slope of the soft mode $S = 8.294 \times 10^{20}$/K (sec)^2. Since $\alpha_0 = mS$, we obtain the following values for these three constants:

$$T_c = 120 \text{ K}, \quad T_0 = 125 \text{ K}, \quad \alpha_0 = 7.6587 \times 10^{23} \ \frac{\text{J}}{\text{m}^5 \text{ kg K}}.$$

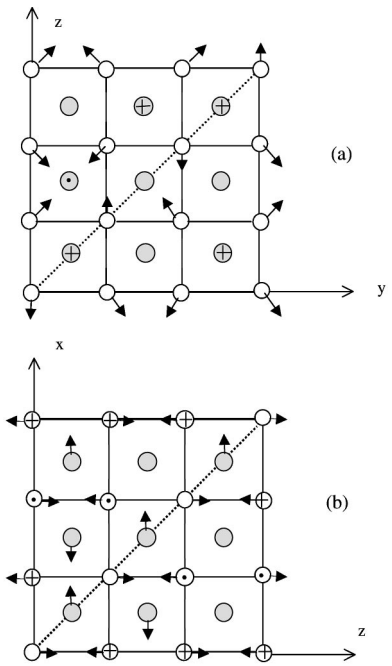

FIG. 8. Illustration of lattice displacement pattern in two different antiphase structures with the APB oriented along [101] and [011], respectively.

The nonlinear expansion coefficients B and C can be determined by the temperature dependence of structural data.[17] At the transition temperature, we can relate the value of the order parameter to the Landau free-energy coefficients: $Q_c^2 = 3B/4C$ and $\alpha_0(T_c - T_0) = 3B^2/16C$. Thus, we find

$$B = \frac{4\alpha_0(T_c - T_0)}{Q_c^2}, \quad C = \frac{3\alpha_0(T_c - T_0)}{Q_c^4}.$$

Specifically, by comparing with the atomic displacements measured for the tetragonal phase, the two model parameters (Q_c, ζ) may be determined from the two atomic displacements ϵ and δ for La and $Ag_{1-x}In_x$, respectively, according to

$$Q_c = \sqrt{2}\sqrt{M_1(2a_t\delta)^2 + M_2(c_t\epsilon)^2}, \quad \zeta = \frac{c_t\epsilon}{2a_t\delta}.$$

We find the following values:

$$Q_c^2 = 3.8823 \times 10^{-46} \text{ kg m}^2, \qquad \zeta = 1.010\,45,$$

and

$$B = 3.9455 \times 10^{70} \ \frac{\text{J}}{\text{m}^7(\text{kg})^2}, \quad C = 7.622 \times 10^{115} \ \frac{\text{J}}{\text{m}^9(\text{kg})^3}.$$

Note that the units of α_0, B, and C contain mass (kg) in the denominator since the order parameter, Q in Eq. (1), has units of $(\text{kg})^{1/2}$ m.

TABLE II. Coefficients $A', A'', B_1', B_4', B_1'', B_4''$ and for antiphase boundary between I_x and II_x. Here $e_1^\infty = -(2D_1/\hat{c}_{11})Q_0^2$, $e_2^\infty = [\sqrt{3}(D_2+\sqrt{3}D_3)/\hat{c}_{22}]Q_0^2$, and $e_3^\infty = [(D_2+\sqrt{3}D_3)/\hat{c}_{22}]Q_0^2$.

Wall orientation	A'		
[010]	$D_1e_1^\infty - 2(D_2+\sqrt{3}D_3)e_3^\infty + \dfrac{[\sqrt{2}D_1-2(D_2-\sqrt{3}D_3)](\sqrt{2}D_1+D_2+\sqrt{3}D_3)}{\hat{c}_{11}+2\hat{c}_{22}}Q_0^2$		
[100]	$D_1e_1^\infty - 2(D_2+\sqrt{3}D_3)e_3^\infty + \dfrac{[\sqrt{2}D_1-2(D_2+\sqrt{3}D_3)]^2}{\hat{c}_{11}+2\hat{c}_{22}}Q_0^2$		
[011]	$D_1e_1^\infty - 2(D_2+\sqrt{3}D_3)e_3^\infty + \dfrac{2(\sqrt{2}D_1+D_2+\sqrt{3}D_3)^2}{2\hat{c}_{11}+\hat{c}_{22}+6\hat{c}_{44}}Q_0^2$		
[101]	$D_1e_1^\infty + \dfrac{2D_1^2}{\hat{c}_{11}+3\hat{c}_{44}}Q_0^2$		
Wall orientation	A''		
[010]	$D_1e_1^\infty - 2(D_2+\sqrt{3}D_3)e_3^\infty + \dfrac{(\sqrt{2}D_1+4D_2)(\sqrt{2}D_1+D_2+\sqrt{3}D_3)}{\hat{c}_{11}+2\hat{c}_{22}}Q_0^2$		
[100]	A'		
[011]	A'		
[101]	A'		
Wall orientation	B_1'	B_4'	
[010]	$-\dfrac{(\sqrt{2}D_1-2D_2+2\sqrt{3}D_3)^2}{4(\hat{c}_{11}+2\hat{c}_{22})}$	$\dfrac{[\sqrt{2}D_1-2(D_2-\sqrt{3}D_3)](\sqrt{2}D_1+4D_2)}{2(\hat{c}_{11}+2\hat{c}_{22})}$	
[100]	$-\dfrac{[(\sqrt{2}D_1-2(D_1+2\sqrt{3}D_3)]^2}{4(\hat{c}_{11}+2\hat{c}_{22})}$	$2B_1'$	
[011]	$-\dfrac{2(\sqrt{2}D_1+D_2+D_3)^2}{2(2\hat{c}_{11}+\hat{c}_{22}+6\hat{c}_{44})} - \dfrac{(\sqrt{3}D_2-D_3)^2}{\hat{c}_{22}}$	$-\dfrac{2(\sqrt{2}D_1+D_2+D_3)^2}{(2\hat{c}_{11}+\hat{c}_{22}+6\hat{c}_{44})} + \dfrac{(\sqrt{3}D_2-D_3)^2}{\hat{c}_{22}}$	
[101]	$-\dfrac{D_1^2}{2(\hat{c}_{11}+3\hat{c}_{44})} + \dfrac{(D_2+\sqrt{3}D_3)^2}{2\hat{c}_{22}}$	$2B_1'$	
Wall orientation	B_1''	B_4''	
[010]	$-\dfrac{(\sqrt{2}D_1+4D_2)^2}{4(\hat{c}_{11}+2\hat{c}_{22})}$	B_4'	
[100]	B_1'	B_4'	
[011]	B_1'	B_4'	
[101]	B_1'	B_4'	

B. Gradient terms and phonon dispersion

The gradient coefficients are related to the curvature of the dispersion surface near the soft mode[24] and the dispersion relation can be measured by inelastic neutron-scattering experiments.

Starting with the Euler-Lagrange equation with explicit time dependence,

$$m\ddot{Q}_\lambda + \frac{\partial(F_L+F_G)}{\partial Q_\lambda} - \sum_j \frac{\partial}{\partial x_j}\left(\frac{\partial F}{\partial Q_{\lambda,j}}\right) = 0 \quad (\lambda = 1-6, j = 1-3), \tag{20}$$

where m is the effective-mass density of atoms associated with the M_5^- mode. For small amplitude oscillations, we can

ignore the nonlinear terms by keeping only the lowest-order terms in the order parameter. Thus, the above six linearized equations have the following harmonic solutions: $Q_\lambda = Q_\lambda^0 \exp[i(\vec{k}_M \cdot \vec{x} - \omega t)]$, where $\mathbf{k}_M$ is one of the arms of the star $\mathbf{k}_M^*$. The M_5^- mode is sixfold-degenerate and it splits into several distinct modes if the $\mathbf{k}$ value deviates from that at the first Brillouin-zone edge. For example, if $\mathbf{k}=\mathbf{k}_M-\mathbf{q}$, then Eq. (20) results in the following eigenvalue problem:

$$m\omega^2 \mathbf{Q} = G\mathbf{Q}, \tag{21}$$

where

$$G = \begin{pmatrix} G_1 & 0 & 0 \\ 0 & G_2 & 0 \\ 0 & 0 & G_3 \end{pmatrix}, \tag{22a}$$

and the 2×2 G_i matrices are given by

$$G_1 = \begin{pmatrix} 2A+2g_1q_1^2+2g_2q_2^2+2g_3q_3^2 & (g_4+g_5)q_1q_2 \\ (g_4+g_5)q_1q_2 & 2A+2g_2q_1^2+2g_1q_2^2+2g_3q_3^2 \end{pmatrix}, \tag{22b}$$

$$G_2 = \begin{pmatrix} 2A+2g_2q_1^2+2g_3q_2^2+2g_1q_3^2 & (g_4+g_5)q_1q_3 \\ (g_4+g_5)q_1q_3 & 2A+2g_1q_1^2+2g_3q_2^2+2g_2q_3^2 \end{pmatrix}, \tag{22c}$$

$$G_3 = \begin{pmatrix} 2A+2g_3q_1^2+2g_1q_2^2+2g_2q_3^2 & (g_4+g_5)q_2q_3 \\ (g_4+g_5)q_2q_3 & 2A+2g_3q_1^2+2g_2q_2^2+2g_1q_3^2 \end{pmatrix}. \tag{22d}$$

The matrix G is in block-diagonal form and the three blocks are equivalent when we choose different arms of the star $\mathbf{k}_M$. The gradient energy causes the two coupled modes of a given $\mathbf{k}$ value to split when moving away from the M point. We can use one of the blocks in G to derive the dispersion relations by introducing a small perturbation to the wave vector along the high-symmetry directions in the first Brillouin zone. Let us choose the first block G_1, which involves the order-parameter components Q_1 and Q_2 and the wave vector $\mathbf{k}=2\pi/a[110]$.

In the M-Γ direction, the perturbation is $\mathbf{q}=q[1,1,0]$ with the amplitude $q \ll 2\pi/a$. The perturbation causes mode splitting:

$$m\omega_1^2 = 2A + (2g_1+2g_2+g_4+g_5)q^2, \tag{23a}$$

$$m\omega_2^2 = 2A + (2g_1+2g_2-g_4-g_5)q^2. \tag{23b}$$

In the M-X direction of the Brillouin zone, $\mathbf{q}=q[010]$ and we can get two more relations:

$$m\omega_3^2 = 2A + 2g_2q^2, \tag{24a}$$

$$m\omega_4^2 = 2A + 2g_1q^2. \tag{24b}$$

Finally, in the M-R direction, $\mathbf{q}=q[001]$, we get

$$m\omega_5^2 = 2A + 2g_3q^2. \tag{24c}$$

Since below the transition temperature $A<0$, phonon stability requires that the slopes of the above five dispersion curves be positive. These five equations give us enough combinations to derive all five independent gradient coefficients g_i in Eq. (3d). However, the phonon dispersions along the M-X and M-R directions have not been measured for $LaAg_{1-x}In_x$.[16–18] Therefore, we can obtain only the two combinations g_1+g_2 and g_4+g_5 by fitting the 300-K data in the M-Γ direction [Fig. 4 (left column, middle panel)] for the longitudinal acoustic (LA) mode for LaAg in Ref. 18 to Eq. (23a) and Fig. 5 for the second transverse acoustic mode (T_2A) for $LaAg_{1-x}In_x$ in Ref. 18 to Eq. (23b). If we denote the slopes for these two dispersions, respectively, by

$$S_1 = 2(g_1+g_2)+(g_4+g_5), \quad S_2 = 2(g_1+g_2)-(g_4+g_5),$$

we find $S_1 = 2.2539\times 10^9$ J/m^3 and $S_2 = 2.1747\times 10^9$ J/m^3. Thus, the two combinations of gradient coefficients are

$$g_1+g_2 = \tfrac{1}{4}(S_1+S_2) = 1.107\,15\times 10^9 \frac{\mathrm{J}}{\mathrm{m}^3},$$

$$g_4+g_5 = \tfrac{1}{2}(S_1-S_2) = 3.96\times 10^7 \frac{\mathrm{J}}{\mathrm{m}^3}.$$

Note that we can determine the temperature dependence of S_2, since the temperature dependence of phonon dispersion for the TA branch of Σ_2 symmetry has also been measured (Fig. 5 in Ref. 18). As discussed above and depicted in Fig. 5, the thickness of the antiphase boundaries is proportional to the square root of the gradient coefficients. The thickness can be on the order of a fraction of a unit cell to several unit-cell dimensions. Unfortunately, there are insufficient data to determine each gradient coefficient and thus the value for parameter d in Eq. (18g), which determines the domain-wall thickness.

VI. SUMMARY AND CONCLUSIONS

Using a Ginzburg-Landau model with a six-dimensional phonon order parameter, we provide, a general formulation of the antiphase structures of $RAg_{1-x}In_x$ (where R = La, Ce,

and Pr) that can form in a cubic ($O_h^1, Pm\bar{3}m$) to tetragonal (D_{4h}^{17}, $I4/mmm$) improper ferroelastic phase transition driven by the M_5^- zone boundary mode of the CsCl structure. There are four independent domain states for each of the three possible tetragonal axes in the low-temperature phase, constituting 12 domain states in total.

Antiphase boundaries are formed between any two domain states of the same tetragonal axis. Using the quasi-1D approximation, we treated four differently oriented APBs and found that equilibrium conditions for the OP profiles can be related to a single set of two dimensionless coupled differential equations involving two components of the OP. The relationships between the parameters in the common set of equations [Eq. (17)] and the free-energy expansion coefficients in Eq. (3) were derived for the case of the tetragonal axis along the *x* direction. These results are also applicable to the cases with the tetragonal axis along the *y* and *z* directions.

It is interesting to note that all of the final differential equations reduce to the same universal set of equations with proper normalization constants. This is also true for other systems that can be described by a Ginzburg-Landau model, although the order parameter may be different. As shown previously for a first-order ferroelectric phase transition,[11] the order parameter is only a three-dimensional vector; the APB solution in that case can also be described by the same set of equations as given in Eq. (17). It is speculative but these equations may be a representative form for all APB domain walls in other transitions

Some of the expansion coefficients in the GL model, Eq. (3), can be extracted from experimental measurements. In particular, we derived the coefficients of the effective Landau free energy and the relationships between the gradient coefficients and the phonon-dispersion curves near the M_5^- soft mode. Note that the analysis presented here is applicable to the cubic to orthorhombic (D_{2h}^5, $Pmma$) transition (see second entry in Table 7 of Ref. 14) in AuCd and NiTi-M ($M=$Fe,Al,Cu) shape memory alloys.[25,26]

ACKNOWLEDGMENTS

We are grateful to Professor G. R. Barsch for numerous insightful discussions and suggestions. This work was supported in part by NSF Grant No. DNS9704714 and in part by the U.S. Department of Energy under Contract No. W-7405-ENG-36.

*Electronic address: cao@math.psu.edu
†Electronic address: avadh@lanl.gov
‡Electronic address: hatchd@wigner.byu.edu

[1] L.D. Landau, Phys. Z. Sowjetunion **11**, 26 (1937); **11**, 545 (1937); *Collected Papers* (Pergamon, London, 1965).
[2] J.-C. Tolédano and P. Tolédano, *The Landau Theory of Phase Transitions* (World Scientific, Singapore, 1987).
[3] A.F. Devonshire, Philos. Mag. **40**, 1040 (1949).
[4] V.L. Ginzburg and L.D. Landau, Zh. Eksp. Teor. Fiz. **20**, 1064 (1950).
[5] G.A. Smolenskii, V.A. Bokov, V.A. Isupov, N.N. Krainik, R.E. Pasynkov, and A.I. Sokolov, *Ferroelectrics and Related Materials* (Gordon and Breach, New York, 1984).
[6] G.R. Barsch and J.A. Krumhansl, Phys. Rev. Lett. **53**, 1069 (1984); Metall. Trans. A **19**, 761 (1988).
[7] A.E. Jacobs, Phys. Rev. B **31**, 5984 (1985).
[8] R.J. Gooding and M.B. Walker, Phys. Rev. B **36**, 5377 (1987).
[9] R.J. Gooding and J.A. Krumhansl, Phys. Rev. B **38**, 1695 (1988).
[10] W. Cao and G.R. Barsch, Phys. Rev. B **41**, 4334 (1990).
[11] W. Cao and L.E. Cross, Phys. Rev. B **44**, 5 (1991); Ferroelectrics **157**, 19 (1994).
[12] V. Janovec, Czech. J. Phys., Sect. B **22**, 974 (1972).
[13] H.T. Stokes and D.M. Hatch, Phys. Rev. B **30**, 4962 (1984); *Isotropy Subgroups of the 230 Crystallographic Space Groups* (World Scientific, Singapore, 1988).
[14] A. Saxena, G.R. Barsch, and D.M. Hatch, Phase Transitions **46**, 89 (1994).
[15] ISOTROPY is a computer program by H. T. Stokes and D. M. Hatch based upon space group representations and parametric distortions which lead to a symmetry reduction. It was used to obtain the data in the tables of Ref. 14. It has been extended to calculate data pertaining to transitions in solids, e.g., domains and their orientations, tensorial properties, gradient invariants, etc.
[16] W. Assmus, R. Takke, R. Sommer, and B. Lüthi, J. Phys. C **11**, L575 (1978).
[17] J. Maetz, M. Müllner, H. Jex, W. Assmus, and R. Takke, Z. Phys. B: Condens. Matter **37**, 39 (1980).
[18] K. Knorr, B. Renker, W. Assmus, B. Lüthi, R. Takke, and H.J. Lauter, Z. Phys. B: Condens. Matter **39**, 151 (1980).
[19] D.M. Hatch, P. Hu, A. Saxena, and G.R. Barsch, Phys. Rev. Lett. **76**, 1288 (1996).
[20] W. Cao, Ph. D. thesis, The Pennsylvania State University, 1987.
[21] A.M. Abakumov, O.I. Lebedev, L. Nistor, G. Van Tendeloo, and S. Amelinckx, Phase Transitions **71**, 143 (2000).
[22] A.M. Abakumov, R.V. Shpanchenko, O.I. Lebedev, G. Van Tendeloo, S. Amelinckx, and E.V. Antipov, Acta Crystallogr., Sect. A: Found Crystallogr. **A55**, 828 (1999).
[23] K. Parlinski and Y. Kawazoe, J. Mater. Res. **12**, 2366 (1997).
[24] W. Cao, J. Phys. Soc. Jpn. **63**, 1156 (1994).
[25] T. Ohba, Y. Emura, S. Miyazaki, and K. Otsuka, Mater. Trans., JIM **31**, 12 (1990).
[26] G.R. Barsch, T. Ohba, and D.M. Hatch, Mater. Sci. Eng., A **275**, 161 (1999).